DOI: 10.61782/fa.2025.0587

FORUM ACUSTICUM EURONOISE 2025

Multi-Channel Acoustic Switch via Activation of Evanescent or Propagation Bloch Wave Modes

Heow Pueh Lee* **Kian Meng Lim** **Yapeng Li**
Department of Mechanical Engineering, National University of Singapore, Singapore

ABSTRACT*

Sonic crystals exhibit interesting phenomena, enabling flexible manipulation of acoustic waves. By leveraging the complex band structure, we propose a wave profile decomposition method to quantitatively predict wave propagation behaviors, revealing that acoustic wave attenuation is influenced by the sound source profile. While earlier studies have demonstrated the feasibility of acoustic switches, the realization of an adjustable multi-channel switch remains unexplored. To address this, a unit cell featuring five Helmholtz resonators is designed to modify sound source profiles by adjusting the orientations of the resonators. This unit cell is connected to three one-dimensional sonic crystals with cylindrical cores to form a multichannel acoustic switch. The ON state of a channel is achieved by activating propagating Bloch wave modes, whereas the OFF state corresponds to the activation of evanescent Bloch wave modes. To enable switching functionality across different frequencies, the orientations of the Helmholtz resonators are optimized to produce desired acoustic source profiles at the outputs. Both experimental and numerical investigations confirm the switching mechanism arising from the activation of evanescent and propagating Bloch wave modes, offering a versatile and tunable platform for advanced acoustic control.

Keywords: *complex band structure, Bloch wave modes, sonic crystal, acoustic switch.*

*__Corresponding author__: mpeleehp@nus.edu.sg.

1. INTRODUCTION

Switches and rectification devices constitute essential components for managing energy flow in various applications, including acoustics and vibration control systems. Different operational principles have been explored to design efficient acoustic or vibration switches.
Based on nonlinear mechanism, Boechler et al. demonstrated an acoustic switching and rectification approach using a one-dimensional granular crystal featuring a defect positioned near one end. By exploiting nonlinear Hertzian contact, which induces bifurcations and chaos, vibration energy originating from frequencies within band gaps is redistributed into lower frequencies within the granular crystal's propagation band [1]. Similarly, Li et al. introduced an acoustic switch based on a driven chain of spherical particles exhibiting nonlinear contact forces, where the output signal is modulated by adjusting the amplitude of a low-frequency control wave [2]. Devaux et al. developed a one-way acoustic switch employing acoustic radiation pressure effects at a water-air interface, effectively controlling directional acoustic propagation [3]. Vanhille and Campos-Pozuelo designed a three-channel acoustic switch based on bubbly-liquid channels. In this mechanism, acoustic waves traveling through the bubbly-liquid medium experience significant attenuation due to the presence of bubbles. By strategically positioning acoustic pressure antinodes to relocate bubbles away from the propagation path, acoustic energy can selectively pass through bubble-free channels [4]. Alagoz et al. proposed another approach, utilizing destructive interference between control waves and input waves, thereby facilitating wave-to-wave acoustic switching [5].
The closure of a sonic crystal (SC) band gap can facilitate the transition from an OFF state to an ON state. For instance, Zhu proposed an acoustic wave switch based on phononic crystals with meta-fluid inclusions that were constructed by alternately stacking sound-hard sub-layers. By altering the orientation of these sub-layers, the anisotropic density of the inclusions is modified, and the opened band gap induces an OFF state in the meta-fluid

phononic crystals [6]. Similarly, Babaee et al. employed an array of elastomeric helices in air; in its undeformed configuration, the system exhibits distinct band gaps characterized by strong wave attenuation. When the helices are axially stretched, these band gaps are suppressed, thereby allowing sound to propagate [7]. In another approach, Bilal et al. realized a phononic transistor-like device by utilizing magnetic coupling to adjust the band gap frequency [8]. Cao et al. designed a Kirigami metashell featuring Archimedean spirals, where deformation of the spiral branches closes the band gap, thus switching the metashell to an ON state [9]. Xue et al. introduced an acoustic switch based on a compressible p-type triply periodic minimal surface structure that can be deformed to either open or close the band gap, thereby controlling the OFF or ON state [10]. Finally, Jia-Hao He et al. [11] developed a bidirectionally tunable, multiconfiguration acoustic diode that controls its ON and OFF states by varying the orientation of square scatterers, and Yuanyuan et al. designed a tunable soft chiral-ligament phononic crystal where unit cell deformations adjust the band gaps [12].

2. DEPENDENCE OF TRANSMISSION LOSS ON SOUND SOURCE PROFILE

In this section, we quantitatively examine the relationship between wave attenuation behaviors, the sound source profile and the complex band structure. A one-dimension SC is studied in the following. The one-dimensional SC under investigation consists of a channel filled with air (density: ρ=1.23 kg/m³, sound speed: c=343 m/s) and N periodically arranged rigid cylinders with a radius of r=15 mm. The channel's width is w=60 mm. Figure 1 (a) illustrates the unit cell of the SC, demonstrating periodicity along the x-axis with a lattice constant of a= 60 mm. Sound hard walls are enforced on the upper and lower sides, and Bloch-Floquet periodic boundary conditions are imposed on the left and right boundaries of the unit cell. Figure 1 (b) shows the complex band structure. The influence of the sound source profiles on wave propagation behaviors are studied. The first three Bloch wave modes at 3.0 kHz are illustrated in the left panels of Figure 1 (c). In the right panel of Figure 1 (c), '+' represents that the phase of sound source is π/2 rad and '−' represents that the phase is -π/2 rad. The contours represent the acoustic pressure fields when the SC is excited by these sound sources. The sound source profile is adjusted according to the Bloch wave modes on the left panel. The resulting acoustic pressure fields in the first cell of the SCs (as shown in the right panels of Figure 1 (c)) closely resemble the Bloch wave modes depicted in the left panels.

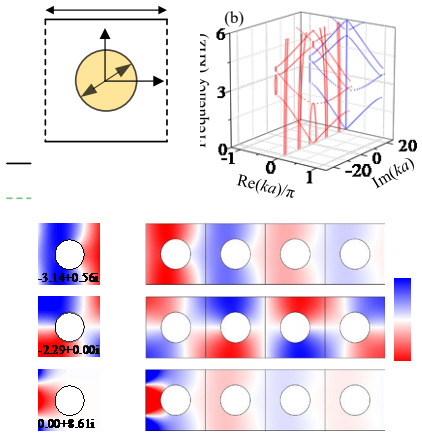

Figure 1. (a) Schematic of the unit cell. (b) Complex band structure. (c) Complex band structure in the Re (ka)-frequency plane (left panel) and Im(ka)-frequency plane (right panel). (c) The first three Bloch wave modes at 3.0 kHz and acoustic pressure fields for three different cases of sound source. The number on the downside of the left panel denotes the value of ka.

Figure 1 (c) demonstrates the feasibility of activating different Bloch wave modes by adjusting the profile of the sound source. Activating a propagating Bloch wave mode enable a large acoustic pressure at the other end of the SC. After sorting the eigen wavenumbers in descending order based on their imaginary part, the m-th order Bloch wave mode can be defined as the mode associated with the m-th eigen wavenumber. Assuming the m-th order Bloch wave mode participates in wave propagation, the acoustic pressure profiles on the left and right boundaries of the unit cell are represented by $p_{m,\mathrm{L}}(y)$ and $p_{m,\mathrm{R}}(y)$, respectively. According to the Bloch-Floquet periodic boundary condition, $p_{m,\mathrm{R}} = p_{m,\mathrm{L}} \exp(-\mathrm{i}k_m a)$ (a is the lattice constant, k_m is the m-th eigen wavenumber). Suppose that a prescribed acoustic pressure is applied on the left boundary of a one-dimensional SC and the profile is $p_{\mathrm{S}}(y)$, this sound source profile can be decomposition into the profiles ($p_{m,\mathrm{L}}(y)$ and (m=1,2,⋯, M)) from different order of Bloch wave modes, expressed as:

$$p_{\mathrm{S}} = p_{\mathrm{L}}^{(1)} = \sum_{m=1}^{M} w_{1,m} p_{m,\mathrm{L}}\,, \tag{1}$$

where $p_{\mathrm{L}}^{(1)}$ represent the acoustic pressure profile on the left boundary of the first unit cell, and M represents that profiles from the first M Bloch wave modes are utilized.

Performing Gram-Schmidt orth-normalization on $p_{m,\mathrm{L}}$ will derive M different basis orthotropic profiles $\hat{p}_{m,\mathrm{L}}$. $p_{m,\mathrm{L}}$ and $\hat{p}_{m,\mathrm{L}}$ are related by:

$$\mathbf{p} = \mathbf{A}\hat{\mathbf{p}}, \tag{2}$$

where $\mathbf{p}$ and $\hat{\mathbf{p}}$ are expressed in column vector forms, expressed as $[p_{1,\mathrm{L}}, p_{2,\mathrm{L}}, ..., p_{M,\mathrm{L}}]^{\mathrm{T}}$ and $[\hat{p}_{1,\mathrm{L}}, \hat{p}_{2,\mathrm{L}}, ..., \hat{p}_{M,\mathrm{L}}]^{\mathrm{T}}$, respectively. $\mathbf{A}$ is a $M \times M$ matrix that transfers orthotropic basis $\hat{p}_{m,\mathrm{L}}$ to basis $p_{m,\mathrm{L}}$ by using Gram-Schmidt orth-normalization, and $A_{i,j} = \langle p_{i,\mathrm{L}}, \hat{p}_{j,\mathrm{L}} \rangle$. According to the Bloch-Floquet periodic boundary condition, the TL can be calculated as:

$$\begin{aligned} \mathrm{TL}^N(\hat{\mathbf{w}}_1) &= -20\log(\left\|\hat{\mathbf{w}}_1\mathbf{A}^{-1}\mathbf{D}^N\mathbf{A}\right\|_2) \\ &= -20\log(\left\|\bar{\mathbf{w}}_1\mathbf{D}^N\mathbf{A}\right\|_2) \end{aligned}, \tag{3}$$

where $\mathrm{TL}^N(\hat{\mathbf{w}}_1)$ represent the TL of a SC with N unit cells and excited by a sound source with a profile of $p_{\mathrm{S}} = \hat{\mathbf{w}}_1\hat{\mathbf{p}}$. In Equation (3), $\|\hat{\mathbf{w}}_1\|_2$ is 1 and $\bar{\mathbf{w}}_1$ is $\hat{\mathbf{w}}_1\mathbf{A}^{-1}$ with $\|\hat{\mathbf{w}}_1\|_2 = 1$.

3. DESIGN METHOD OF THE ACOUSTIC SWITCH

In this section, we propose a design methodology for an acoustic switch. For brevity, the design principle is demonstrated using a single-channel acoustic switch, as illustrated in Figure 2 (a). This configuration comprises a one-dimensional SC with the acoustic switch cell positioned at the left end, where a plane wave is incident. The detailed structure of the acoustic switch is depicted in Figure 2 (b). Central to the switch cell is a C-split resonator—although other scatterer configurations may also be employed—which is characterized by an outer radius of r=15 mm, a thickness (dr) of 2 mm, and a split width of w=2 mm. A plane wave sound source, designated as $p_{\mathrm{in}}(y)$, is applied at the left boundary of the switch cell. As the acoustic waves propagate through the switch cell, the output acoustic pressure profile, $p_{\mathrm{out}}(y)$, is altered. Based on the criteria discussed in Section 2, if $p_{\mathrm{out}}(y)$ excites propagating Bloch wave modes, the acoustic waves continue to propagate through the subsequent SC, thereby placing the switch in the ON state. Conversely, if $p_{\mathrm{out}}(y)$ triggers evanescent Bloch wave modes, the acoustic wave is inhibited from propagating, resulting in an OFF state. By adjusting the orientation (θ) of the C-split resonator, the output acoustic pressure profile can be effectively modulated, thereby controlling the switching state. This approach highlights the feasibility of using geometric and orientation adjustments to achieve tunable acoustic wave manipulation in engineered sonic crystals.

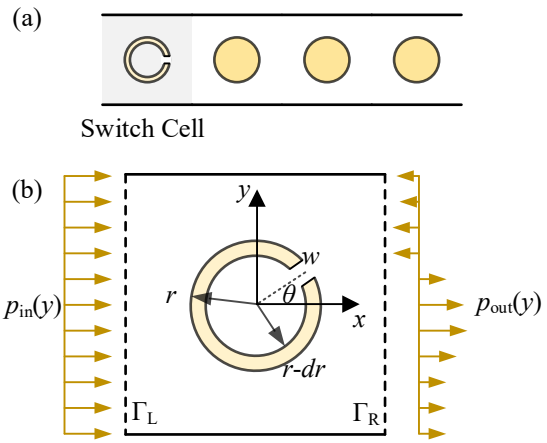

Figure 2. (a) Schematic of the acoustic switch. The cell on the left end is the switch cell. (b) Detail illustration of the switch cell. The switch cell contains a C-split.

According to the design principle—where the activation of evanescent or propagating Bloch wave modes hinges on accurately predicting the output acoustic pressure profile from a given input—the key is to model the wave propagation within the switch cell precisely. Here, we analyze the switch cell illustrated in Figure 2 (b). The left boundary is treated as an acoustic pressure boundary, while the boundaries of the C-split resonator and the upper and lower boundaries are considered sound-hard wall boundaries. Consequently, determining the overall acoustic pressure profile also requires specifying the acoustic boundary condition on the right side (Γ_{R}), which serves as the interface between the switch cell and the sonic crystal. Before defining the precise boundary condition on Γ_{R}, we first examine the acoustic pressure and the normal acoustic velocity at the different interfaces depicted in Figure 3.

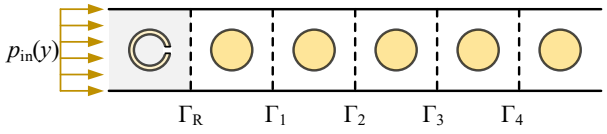

Figure 3. Different interfaces in the acoustic switch.

According to Equation (1), the acoustic pressure and acoustic norm velocity can be decoupled as:

$$p_{\mathrm{R}} = \sum_{m=1}^{M} w_{1,m} p_{m,\mathrm{L}}, \quad v_{\mathrm{R}} = \sum_{m=1}^{M} w_{1,m} v_{m,\mathrm{L}}. \tag{4}$$

After acoustic waves propagate through several unit cells of the sonic crystal, the acoustic pressure and velocity at the

nth interface are characterized by the Bloch-Floquet periodic boundary conditions. The acoustic pressure and velocity can be expressed as follows:

$$\begin{aligned} p_n &= \sum_{m=1}^{M} w_{1,m} p_{m,\mathrm{L}} \exp(-in\,\mathrm{Re}(k_m a)) \exp(-n\,\mathrm{Im}(k_m a)) \\ v_n &= \sum_{m=1}^{M} w_{1,m} v_{m,\mathrm{L}} \exp(-in\,\mathrm{Re}(k_m a)) \exp(-n\,\mathrm{Im}(k_m a)) \end{aligned} . \quad (5)$$

As n increases, the contribution of the evanescent component diminishes, and both the acoustic pressure and acoustic velocity converge to their steady-state values:

$$\begin{aligned} p_n &\approx w_{1,1} p_{1,\mathrm{L}} \exp(-in\,\mathrm{Re}(k_1 a)) \\ v_n &\approx w_{1,1} v_{1,\mathrm{L}} \exp(-in\,\mathrm{Re}(k_m a)) \end{aligned} . \quad (6)$$

This result indicates that the acoustic impedance converges to a constant profile, expressed as:

$$Z = \frac{p_n}{v_n} = \frac{p_{1,\mathrm{L}}}{v_{1,\mathrm{L}}}, \quad (7)$$

where $p_{1,\mathrm{L}}$ is acoustic pressure profile of the propagating Bloch wave mode, and $v_{1,\mathrm{L}}$ is velocity profile of the propagating Bloch wave mode. Hence, we define the propagating Bloch mode impedance as $Z_{\mathrm{PB}} = p_{1,\mathrm{L}} / v_{1,\mathrm{L}}$.

After applying the Bloch mode impedance boundary condition to the right boundary of the switch cell, we can compute the output acoustic pressure profile, $p_{\mathrm{out}}(y)$, for a prescribed input profile. Using Equation (3), the transmission loss (TL) of the acoustic switch can then be determined based on this output pressure profile. To validate the capability of the Propagating Bloch Impedance (PBI) boundary condition in predicting the switch cell's output profile, we examine cases with rotation angles of 0° and 90°. In both scenarios, different SC unit cells are analyzed, as depicted in Figure 4 (a) and Figure 4 (c). Figure 4 (b) and Figure 4 (d) present a comparison between the TL calculated via Equation (3) and that obtained from the commercial software COMSOL. The strong correlation between these results indicates that the PBI boundary condition reliably predicts the output acoustic profile and that the predictive model based on Equation (3) accurately estimates the TL.

Next, we determine the rotation angle of the acoustic switch by solving the following optimization problem:

$$\begin{aligned} \min_{\theta_{\mathrm{ON}},\theta_{\mathrm{OFF}}} \quad & \mathrm{TL}(\theta_{\mathrm{ON}}, f_0) - \mathrm{TL}(\theta_{\mathrm{OFF}}, f_0) \\ s.t. \quad & \theta_{\mathrm{ON}}, \theta_{\mathrm{OFF}} \in [0,\, 180^\circ] \end{aligned} . \quad (8)$$

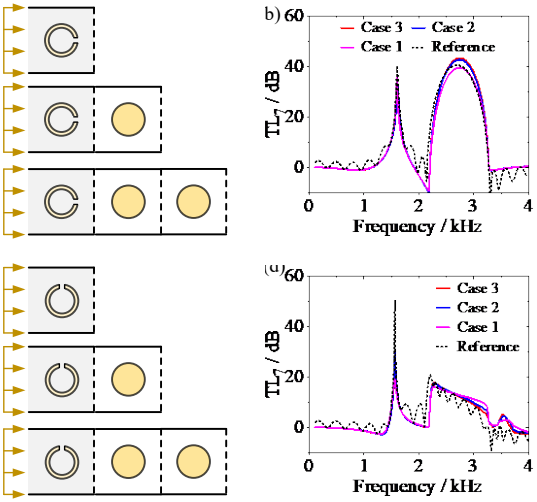

Figure 4. (a) Numerical model to calculate the output acoustic pressure profile $p_{\mathrm{out}}(y)$ of the switch cell when the rotation angle θ is 0°. (b) Comparison of the TL calculated with predicated pressure profile $p_{\mathrm{out}}(y)$ and reference from COMSOL (θ is 0°). (c) Numerical model to calculate the output acoustic pressure profile $p_{\mathrm{out}}(y)$ of the switch cell when the rotation angle θ is 90°. (d) Comparison of the TL calculated with predicated pressure profile $p_{\mathrm{out}}(y)$ and reference from COMSOL. (θ is 90°). PBI indicates propagating Bloch impedance boundary condition. Case 1, 2, and 3 indicates there are zero, one or two unit cells of SC in the prediction model.

where θ_{ON} and θ_{OFF} is the rotation angle when the switch is in ON state and OFF state, respectively. f_0 is working frequency. By setting f_0 as 3.0 kHz, and solving Equation (8) with the PSO algorithm, we derive that θ_{ON} is 100.7°, and θ_{OFF} is 0°. Figure 5 shows the acoustic pressure field when the rotation angle is in OFF (upper panel) state or ON (lower panel) state.

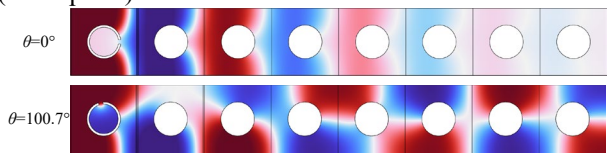

Figure 5. Acoustic pressure of the acoustic switch when the rotation angle is θ_{OFF}= 0° (upper panel) and is θ_{ON}= 100.7° (lower panel).

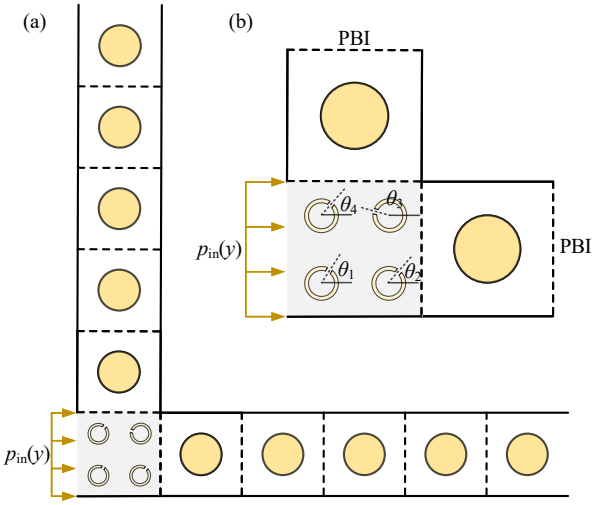

Figure 6. (a) Two-channel acoustic switch. (b) Numerical model to predict the output acoustic pressure profile and TL.

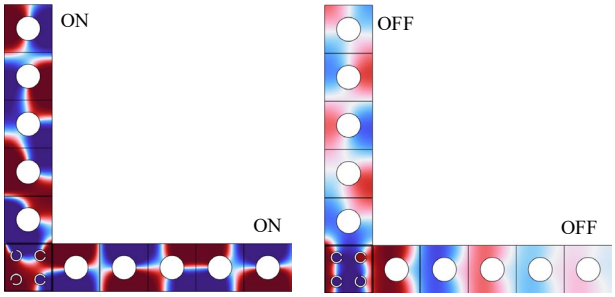

Figure 7. Acoustic pressure of the acoustic switch when both branches are in ON state (left panel with **θ**=[209.6°, 0°, 0°, 107.5°]) or OFF state (right panel with **θ**=[0°, 102.87°, 0°, 0°]).

For a multichannel acoustic switch, as illustrated in Figure 6 (a), Figure 6 (b) shows the corresponding numerical model used to predict the acoustic pressure profiles. In the switch unit cell, four C-split resonators with individually adjustable rotation angles are employed. By varying the orientations of these resonators, the output acoustic pressure profiles directed to the upper sonic crystal (SC) and the left SC can be independently controlled. Here, TL_U represents the transmission loss of the upper SC branch, while TL_L represents the transmission loss of the left branch. To simultaneously control both branches such that they are in the same ON or OFF state, the following optimization problem can be formulated:

$$\begin{aligned} \min_{\theta_{ON},\theta_{OFF}} \quad & \left[\mathrm{TL_L}(\boldsymbol{\theta}_1, f_0) - \mathrm{TL_L}(\boldsymbol{\theta}_2, f_0)\right] \\ & + \left[\mathrm{TL_U}(\boldsymbol{\theta}_1, f_0) - \mathrm{TL_U}(\boldsymbol{\theta}_2, f_0)\right] \\ s.t. \quad & \boldsymbol{\theta}_1 = [\theta_{1,1}, \theta_{1,2}, \theta_{1,3}, \theta_{1,4}] \in [0, 360^\circ] \\ & \boldsymbol{\theta}_2 = [\theta_{2,1}, \theta_{2,2}, \theta_{2,3}, \theta_{2,4}] \in [0, 360^\circ] \end{aligned}, \tag{9}$$

And the design results in shown in Figure 7.

To derive a double-channel switch that one is in ON state and the other is in OFF state, we define he optimization problem as follows:

$$\begin{aligned} \min_{\theta_{ON},\theta_{OFF}} \quad & \left[\mathrm{TL_L}(\boldsymbol{\theta}_1, f_0) - \mathrm{TL_L}(\boldsymbol{\theta}_2, f_0)\right] \\ & + \left[\mathrm{TL_U}(\boldsymbol{\theta}_2, f_0) - \mathrm{TL_U}(\boldsymbol{\theta}_1, f_0)\right] \\ s.t. \quad & \boldsymbol{\theta}_1 = [\theta_{1,1}, \theta_{1,2}, \theta_{1,3}, \theta_{1,4}] \in [0, 360^\circ] \\ & \boldsymbol{\theta}_2 = [\theta_{2,1}, \theta_{2,2}, \theta_{2,3}, \theta_{2,4}] \in [0, 360^\circ] \end{aligned}, \tag{10}$$

And the design results in shown in Figure 8.

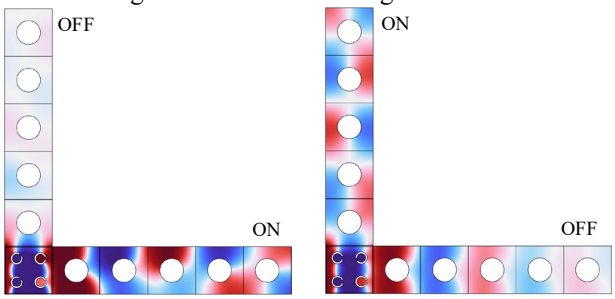

Figure 8. Acoustic pressure of the acoustic switch when the two branches have opposite states. Left panel with **θ**=[42.9°, 0°, 0°, 41.9°] and right panel with **θ**=[0°, 0°, 198.5°, 0°]).

4. ACKNOWLEDGMENTS

The authors would like to acknowledge the financial support from the Ministry of Education MOE Tier 2 grant with the project ID MOE-T2EP50221-0007.

5. REFERENCES

[1] N. Boechler, G. Theocharis, and C. Daraio: "Bifurcation-based acoustic switching and rectification," *Nature materials*, vol. 10, no. 9, pp. 665-668, 2011.

[2] F. Li, P. Anzel, J. Yang, P. G. Kevrekidis and C. Daraio: "Granular acoustic switches and logic elements," *Nature communications*, vol. 5, no. 1, pp. 5311, 2014.

[3] T. Devaux, A. Cebrecos, O. Richoux, V. Pagneux and V. Tournat: "Acoustic radiation pressure for nonreciprocal transmission and switch effects," *Nature Communications*, vol. 10, no. 1, pp.3292, 2019.

[4] C. Vanhille and C. Campos-Pozuelo: "An acoustic switch," *Ultrasonics sonochemistry*, vol. 21, no. 1, pp. 50-52, 2014.

[5] S. Alagoz and B. Baykant Alago: "Sonic crystal acoustic switch device," *The Journal of the Acoustical Society of America*, vol. 133, no. 6, pp. 485-490, 2013.

[6] X. F. Zhu: "Acoustic waves switch based on meta-fluid phononic crystals," *Journal of Applied Physics*, vol. 112, no. 4, pp. 044509, 2012.

[7] S. Babaee, N. Viard, P. Wang, N. X. Fang and K. Bertoldi: "Harnessing deformation to switch on and off the propagation of sound," *Adv. Mater*, vol. 28, no. 8, pp. 1631-1635, 2016.

[8] O.R. Bilal, A. Foehr and C. Daraio: "Bistable metamaterial for switching and cascading elastic vibrations," *Proceedings of the National Academy of Sciences*, vol. 114, no. 18, pp.4603-4606, 2017.

[9] P. Cao, W. Ou, Y. Su, Y. Yin, E. Dong, Z. Song, J. Li and Y. Zhang: "Acoustic switch via kirigami metasurface," *Physical Review Applied*, vol. 18, no. 5, pp. 054040, 2022.

[10] P. Xue, H. Dai and L. Zhou: "Acoustic switch via a compressible minimal surface structure," *Advanced Engineering Materials*, vol. 25, no. 4, pp. 2201144, 2023.

[11] J. H. He and H. H. Huang: "Multiband switching realized by a bidirectionally tunable and multiconfiguration acoustic diode," *AIP Advances*, vol. 8, no. 10, pp.105032, 2018.

[12] Y. Li, K. Huang, M. Gong, C. Sun, S. Gao, Y. Lai and X. Liu: "Realization of acoustic tunable logic gate composed of soft materials," *Results in Physics*, 57, p.107421, 2024.